Microscopic evidence for 4f localization with reduced particle size in correlated electron system $CePd_3$

S. K. Mohanta, S. N. Mishra, Kartik K. Iyer, and E. V. Sampathkumaran
Tata Institute of Fundamental Research (TIFR), Homi Bhabha Road, Mumbai-400005, India
(Received 20 November 2012; published 18 March 2013)

We report the temperature dependence of magnetic hyperfine field, B_{hf}, for ^{111}Cd impurity in nanocrystalline $CePd_3$ measured using the time differential perturbed angular correlation technique. With a reduction of particle size, we find progressive increase in the hyperfine field of Cd which shows Curie-Weiss-like temperature dependence for nanoparticles smaller than 60 nm in size. Supplemented by bulk susceptibility and isothermal magnetization measurements, our data show microscopic evidence for 4f localization in nanoparticles of correlated electron system $CePd_3$.

DOI: 10.1103/PhysRevB.87.125125 PACS number(s): 71.27.+a, 61.46.Hk, 75.20.Hr, 76.80.+y

Effects of crystal size on electronic and magnetic properties of materials is a topic of considerable interest. A reduction of lattice size is known to have strong influence on the physical properties of materials, particularly magnetism.[1–5] While many studies have been carried out in simple metals, alloys, and oxides, much less information is available on size effects in strongly correlated electron systems (SCESs) based on metals containing f electrons. Over the years intermetallic compounds of Ce have been found to show many novel phenomena like valence fluctuation, heavy fermion, etc., essentially arising due to strong electron-electron correlations.[6] Recently size effects have been studied in some Ce based intermetallic compounds.[7–13] While a reduction in particle size has been reported to depress intersite magnetic interaction in many cases[7,8] as though there is a tendency towards 4f delocalization, this scenario is in contradiction with the inference of localization of 4f electrons in reduced dimensions reported from photoemission studies in some Ce compounds.[14] In fact, in support of the latter picture, the size reduction has been reported to result in magnetic ordering at the core of the nanoparticles of some Ce based Kondo lattices.[11–13] Clearly, there is a controversy on this issue. It is therefore important to resolve this issue through a bulk-sensitive microscopic experimental method to advance theoretical understanding of electron correlation effects as a function of size in the field of SCESs of f-electron systems.

In this paper, we address this question through a nuclear method, namely, the time differential perturbed angular correlation (TDPAC).[15–18] For our investigation, we have chosen $CePd_3$, a well-known correlated electron system, which forms in a face-centered-cubic (fcc) crystal structure.[19] In this compound, the Ce-4f electrons are known to be delocalized with unstable magnetic moments characterized by a large spin fluctuation temperature $T_{SF} \geqslant 250$ K.[20–22] Apart from bulk magnetization studies, we have carried out local investigations to understand the magnetism of fine particles of this compound by measuring the hyperfine field of ^{111}Cd using TDPAC spectroscopy. As it is well known that Cd occupies the Ce (cubic) site in this compound,[23] this binary cubic system offers an ideal opportunity to address the issue at hand. Our data reveal a strong influence of particle size on the magnetism of nanocrystalline $CePd_3$. With a reduction of particle size, we find a progressive increase of magnetic susceptibility (χ) and ^{111}Cd hyperfine field, both showing Curie-Weiss-type temperature dependence for small particles (typically smaller than 60 nm). The observed features show conclusive evidence for 4f localization in the correlated electron system $CePd_3$.

Nanocrystalline samples of $CePd_3$ were prepared by high speed ball milling in toluene medium.[12,13] They were characterized by x-ray-diffraction measurements. In addition, scanning and transmission electron microscopic (SEM, TEM) studies were carried out to infer about particle sizes. Compositions were ascertained from energy dispersive x-ray analysis (EDAX). More information about these experimental details can be found elsewhere.[12,13] The bulk magnetic properties of the samples were studied by measuring magnetization as a function of temperature and applied magnetic field using a commercial superconducting quantum interference device magnetometer.

TDPAC measurements were carried out using ^{111}Cd probe, produced via electron capture decay of ^{111}In. The 247 keV, $I = 5/2^+$ level in ^{111}Cd with a half-life of $T_{1/2}$~ = ~84 ns,[24] served as a local probe for the detection of electric and magnetic hyperfine fields. The parent ^{111}In nuclei were produced via the heavy-ion reaction ^{108}Pd(^{7}Li, 4n)^{111}In by bombarding the samples with a 34-MeV ^{7}Li beam. The ^{111}In probes thus produced get implanted in the sample at a depth $\geqslant 1\mu$m and concentration typically less than 1 ppm. Measurements were carried out in the temperature range 20–500 K using an experimental setup consisting of four La(Ce)Br_3 detectors placed at angles $\theta = 0, \pm 90$ and 180°, all in the horizontal plane. To extract the perturbation due to hyperfine interactions, spin rotation spectra are defined as $R(t) = \frac{2[W(180^\circ,t)-W(90^\circ,t)]}{[W(180^\circ,t)+2W(90^\circ,t)]}$, where $W(\theta,t)$ are the background-subtracted normalized coincidence counts of the detector. If Cd nuclei are subjected to quadrupole interaction due to axially symmetric electric-field gradient (EFG), the PAC spectra are expressed as $R(t) = A_{22}[1/5 + \sum_{n=1}^{3}[\cos(n\omega_0 t)e^{-\delta\omega_n t}]$ where A_{22} is the anisotropy of the γ-γ cascade in ^{111}Cd and $\omega_0 = \frac{6eQV_{zz}}{4I(2I-1)\hbar}$ is the fundamental frequency which gives a measure of the principal component V_{zz} of the EFG tensor.[15–17] For magnetic interaction in the presence of transverse external field, the $R(t)$ spectra are expressed by the relation $R(t) = \frac{3}{4}A_{22}e^{-\delta\omega_L t}\cos(2\omega_L t)$. Here, $\omega_L = \hbar^{-1}g_N\mu_N B_{\text{eff}}$ is the Larmor frequency related to the effective magnetic hyperfine field $B_{\text{eff}}(= B_{\text{ext}} + B_{\text{hf}})$ acting on the probe nuclei. The exponential factor accounts for possible damping of the $R(t)$ spectra

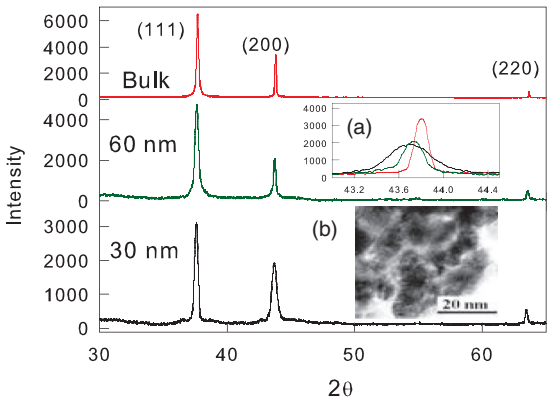

FIG. 1. (Color online) X-ray-diffraction patterns for bulk and nanocrystalline $CePd_3$ obtained by high-speed ball milling. For visual clarity, the vertical scale for the top and middle curves has been shifted by an arbitrary constant. Inset: (a) expanded view of (200) peak, (b) TEM picture of 30-nm sample.

due to local inhomogeneity and/or dynamic spin fluctuation. In paramagnetic systems, the internal field $B_{\rm hf}$ is generally proportional to the applied magnetic field. In such a case, it is convenient to extract the Knight shift $K = B_{\rm hf}/B_{\rm ext}$ which provides a measure of the local spin susceptibility at the probe site.[15–18]

Figure 1 displays the room-temperature x-ray-diffraction patterns observed for bulk and nanocrystalline $CePd_3$. The diffraction patterns could be indexed with $AuCu_3$-type fcc structure with no detectable extra impurity phase. The x-ray lines become broader with increasing milling time, indicating significant reduction of the crystallite size. From the instrument-corrected line broadening of the x-ray lines, the crystallite size of the nanoparticles was determined using the Debye-Scherrer formula.[25] The average particle size for our samples was found to be 150 ± 20 nm, 60 ± 10 nm and 30 ± 5 nm for milling times 1, 2, and 5 h, respectively. The SEM and TEM pictures confirmed the reduction of particle size to this range (see inset in Fig. 1). It is worthwhile to note that the x-ray lines shift towards lower angles as the particle size is reduced. The lattice parameters derived by least-squares fitting of the d spacings was found to be 4.131 Å for bulk $CePd_3$, in agreement with the values reported in the literature.[19] For the nanocrystalline samples the lattice constants were found to be $a = 4.134$, 4.138, and 4.141 Å for particles of sizes 150, 60, and 30 nm, respectively, indicating a marginal expansion of the unit cell with a decrease of the particle size which is distinctly visible if we inspect, for instance, the (200) peak position carefully (see an inset in Fig. 1).

Figure 2 shows $\chi(T)$ behavior of bulk and nano-$CePd_3$ measured in an applied field of 0.5 T. The data for bulk $CePd_3$ show a weak temperature dependence with a broad hump around 150 K in agreement with earlier results.[20,26] The data show a strong upturn below 50 K, which may be due to the onset of coherence as suggested by Lawrence *et al.*[21] With the size reduction, the peak in $\chi(T)$ shifts towards lower temperatures and the data show Curie-Weiss-like behavior for particles smaller than 60 nm. This is more clearly visible in the plot of $1/\chi$ vs T shown in the inset of Fig. 2. For the 60- and 30-nm particles, the data above 100 K could be

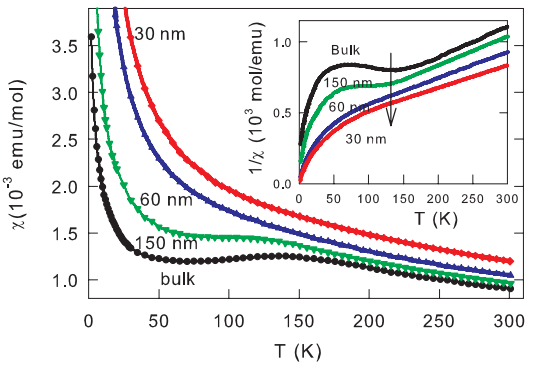

FIG. 2. (Color online) Temperature dependence of magnetic susceptibility for nanocrystalline $CePd_3$ measured in an applied field of 0.5 T. Inset shows the inverse susceptibility as a function of temperature.

fitted to Curie-Weiss (CW) behavior: $\chi(T) = C/(T + \theta_P)$, from which the effective moment $\mu_{\rm eff}$ per formula unit was estimated to be $2.08\,\mu_B$ and $2.24\,\mu_B$, respectively, using the relation $C = N\mu_{\rm eff}^2/3k_B$. For such a fit for bulk $CePd_3$, though difficult because of limited data points available above the peak, an attempt was made for $T \geqslant 200$ K yielding $\mu_{\rm eff} = 1.87\mu_B$. The $\mu_{\rm eff}$ obtained for bulk $CePd_3$ is significantly lower than the value $2.54\,\mu_B$ expected for Ce^{3+} ions, consistent with the high spin fluctuation rate and strong mixed valent behavior of Ce reported earlier.[19–21] Regardless of the uncertainties in the $\mu_{\rm eff}$ value, the susceptibility data clearly show a strong dependence with particle size. To explore this aspect further, we measured the isothermal magnetization of the samples as a function of applied field at different temperatures. The results are shown in Fig. 3. It can be seen that the magnetization data show linear dependence down to 10 K, indicating paramagnetic behavior. The data at 2 K show a curvature typical of a strong paramagnet in high fields. The data shown in Figs. 2 and 3 reveal a progressive increase of magnetization in nanocrystalline $CePd_3$ as the particle size is reduced.

The results presented here qualitatively differ from the observations made by Lin *et al.*,[26] which indicated a decrease in magnetization, attributed to an increase in mixed valence with

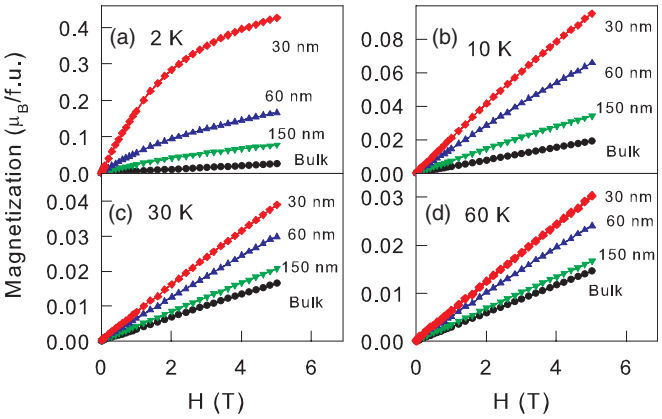

FIG. 3. (Color online) Isothermal magnetization as a function of applied field (M vs H) for bulk and nanocrystalline $CePd_3$ measured at different temperatures. Notations of color are the same for all figures.

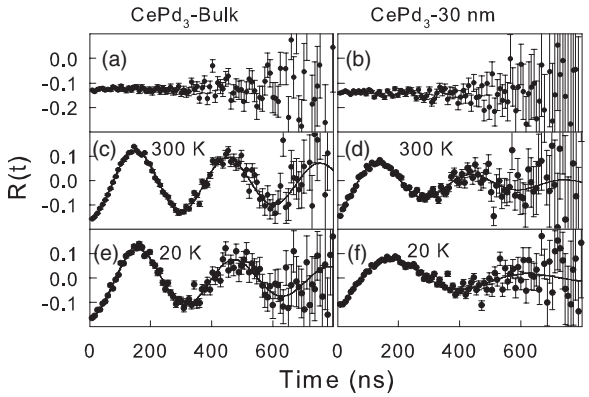

FIG. 4. Typical TDPAC spin rotation spectra of ^{111}Cd in bulk and 30-nm $CePd_3$ recorded in zero applied field (a) and (b) and transverse applied field of 0.7 T (c)–(f).

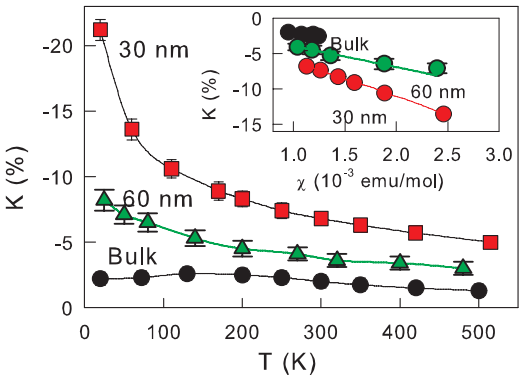

FIG. 5. (Color online) Temperature dependence of ^{111}Cd Knight shift $K = B_{hf}/B_{ext}$ in bulk and nanocrystalline $CePd_3$. Solid lines are guides to the eye. Inset shows the variation of K with bulk susceptibility for temperature range 60–300 K.

reduction of particle size.[26] This is also in contradiction with the results of earlier photoemission studies which indicated enhanced 4 f magnetism in reduced dimensions.[14] A possible reason for the discrepancy may be due to oxidation of samples prepared by laser ablation technique, which is unavoidable due to extreme sensitivity of the nanoparticles of rare earths. In fact, in support of this conjecture, we find that the ball-milled samples also get oxidized as soon as the toluene layer is removed by warming the specimens to about 100 °C in high vacuum and subsequent exposure to air.

Coming to the results of our local magnetic studies in nano-$CePd_3$ by the TDPAC method, it is important to ascertain the lattice location of the probe atoms, which can be inferred from the quadrupole interaction of ^{111}Cd measured without applied field. Figures 4(a) and 4(b) show the zero-field PAC spectra at 300 K. The spectra show high anisotropy with no visible oscillation, indicating the absence of any measurable quadrupole interaction. This suggests that the probes (In/Cd) are located at the Ce site (having cubic symmetry), consistent with the conclusions drawn from recent PAC measurements in RPd_3 (R = rare earth) alloys.[23]

To examine the local magnetic properties of the nanoparticles, measurements were carried out in transverse external magnetic field B_{ext} of 0.7 T. The measured spectra displayed in Figs. 4(c)–4(f) show well-defined oscillations with high amplitude which could be fitted with a single magnetic interaction frequency ω_L. The $R(t)$ spectra for the nanoparticles show considerable damping which increases almost linearly on reducing the sample temperature. The observed damping most likely arises from static inhomogeneous spread in ω_L, caused by the distribution in the particle size. It may also have some contribution from dynamic fluctuation of the Ce magnetic moment. Considering the possible spread in the size of our nanoparticles ($\approx$15%) and the slow oscillation observed in our spectra, it is difficult to separate the contribution from static distribution/dynamic fluctuation. This, however, does not influence the main conclusion of our paper. From the observed ω_L values the Knight shift $K(T) = B_{hf}(T)/B_{ext}$ of ^{111}Cd at different temperatures was extracted. Figure 5 shows the temperature dependence of ^{111}Cd Knight shift in bulk and nano-$CePd_3$. The Knight shift of Cd in bulk $CePd_3$ was found to be small and weakly temperature dependent. Compared to the behavior in bulk $CePd_3$, the results in the nanocrystalline samples show clear-cut differences. First, the magnitude of the Knight shift progressively increases with the reduction of particle size. Second, the $K(T)$ data for the nanoparticles show much stronger temperature dependence, reflecting a Curie-Weiss-like behavior for the sample with particle size smaller than 60 nm.

The Knight shift of a probe nucleus is generally expressed as $K(T) = K_0 + A_{hf}\chi(T)/N\mu_B$, where K_0 is the temperature-independent component related to density of states at the Fermi level $n(E_F)$, A_{hf} is the hyperfine field coupling constant, and N is the Avagadro number.[27] The inset in Fig. 5 displays the plot of Knight shift versus susceptibility for nanocrystalline $CePd_3$. The data show linear dependence for $T \geqslant 100$ K, yielding $A_{hf} = -100$ kG/μ_B, -168 kG/μ_B, and -284 kG/μ_B for bulk, 60- and 30-nm nanoparticles respectively. The corresponding K_0 values were found to increase from -0.2% for bulk $CePd_3$ to -0.9% for 30-nm nanoparticles, indicating a gradual increase of $n(E_F)$ as particle size is reduced. Considering the large implantation depth ($\geqslant 1$ μm) of the probe the observed size-dependent changes in our data cannot arise from the spins near the surface, but genuinely reflect the magnetic response from the bulk of the nanoparticles. This is supported by the large change in bulk magnetic moment, for instance at $H = 50$ kOe (in Fig. 3), which cannot be accounted for by surface atoms alone, as it is well established that the contribution from such an effect is about two orders of magnitude smaller.[28] The hyperfine field data presented here thus provide a clear evidence for an enhancement of magnetic response in nanocrystalline $CePd_3$, consistent with the inference from magnetization data.

To get further insight, we have performed *ab initio* electronic structure calculations within the generalized gradient approximation (GGA) of the density functional theory (DFT)[29] using WIEN2K code[30,31] and experimental values of the lattice parameters for bulk and nano-$CePd_3$. Figure 6 displays the density of states (DOS) obtained from nonmagnetic (unpolarized) calculations. On reduction of particle size, as the unit cell expands, the Ce-4 f band moves closer to Fermi level, resulting in an increase in $n(E_F)$ from 1.8 states/eV in bulk $CePd_3$ to 8.2 states/eV in 30-nm nano-$CePd_3$, which is in agreement with our conclusion arrived from the Knight-shift

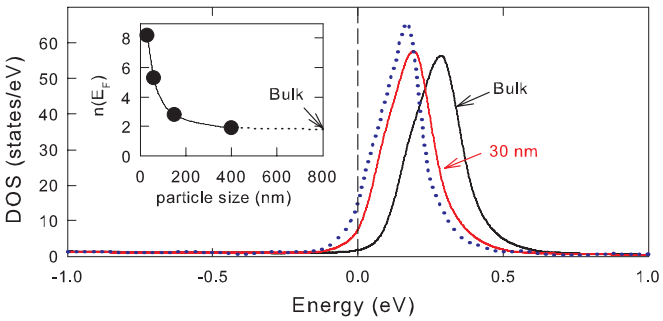

FIG. 6. (Color online) Unpolarized total DOS for bulk and nano-$CePd_3$. Dotted line represents the DOS for the case with defects (see text). The vertical dashed line marks the Fermi energy E_F. Inset shows variation of $n(E_F)$ with particle size.

data. Furthermore, the magnetic moment of Ce, μ_{Ce}, obtained from spin polarized calculations taking account of on-site Coulomb correlation for Ce-f orbitals (GGA+U), was found to increase from nearly zero in bulk $CePd_3$ to $0.57\mu_B$ in 30-nm nano-$CePd_3$. It is worth noting that the magnetic moment on the Pd atoms shows a similar trend with μ_{Pd} increasing from $-0.007\mu_B$ to $0.02\mu_B$ for bulk and nano-$CePd_3$ respectively. The enhanced polarization of Pd coupled with higher Ce-4f moment, that too in closer proximity to the Fermi level, can increase the exchange interaction between Ce moments despite lattice expansion, which explains the trend in the hyperfine field. We would like to note that lattice expansion may not be the sole factor for the observed 4f localization as such a behavior has also been observed in some Ce systems with no change in lattice constants with particle size reduction.[12] In fact, defects intrinsic to nanoparticles alone can play a key role in the magnetic behavior of nanoparticles.[32] To address this point, we have performed calculations using a $2 \times 2 \times 2$ supercell of bulk $CePd_3$ having 8 Ce, 23 Pd, and one vacancy, representing a point defect. The calculation yielded $n(E_F) = 13$ states/eV, $\mu_{Ce} = 0.61\mu_B$ and $\mu_{Pd} \approx 0.03\mu_B$, which are much higher than the results obtained for pristine $CePd_3$. The results obtained from our calculations clearly illustrate that point defects and/or lattice expansion alter the band structure of the nanoparticles causing an increase in $n(E_F)$ which in turn enhances the Ce-4f local moment in nano-$CePd_3$.

In summary we have carried out bulk magnetization and hyperfine interaction studies in nanocrystalline $CePd_3$. The progressive increase of magnetic response with particle size reduction as revealed by macroscopic magnetization studies and Knight-shift measurements of ^{111}Cd nuclei show conclusive microscopic evidence for localization of 4f electrons as the particle size is reduced for the correlated electron system $CePd_3$.

[1] W. P. Halperin, Rev. Mod. Phys. **58**, 533 (1986).
[2] S. D. Bader, Rev. Mod. Phys. **78**, 1 (2006).
[3] F. J. Himpsel, J. E. Ortega, G. J. Mankey, and R. F. Wills, Adv. Phys. **48**, 511 (1998).
[4] S. N. Mishra, S. Bose, P. Vasa, and P. Ayyub, Phys. Rev. B **71**, 094429 (2005).
[5] S. N. Mishra, S. K. Mohanta, S. M. Davane, N. Kulkarni, and Pushan Ayyub, Phys. Rev. Lett. **105**, 147203 (2010).
[6] G. R. Stewart, Rev. Mod. Phys. **73**, 797 (2001).
[7] Y. Y. Chen, Y. D. Yao, C. R. Wang, W. H. Li, C. L. Chang, T. K. Lee, T. M. Hong, J. C. Ho, and S. F. Pan, Phys. Rev. Lett. **84**, 4990 (2000).
[8] S.-W. Han, C. H. Booth, E. D. Bauer, P. H. Huang, Y. Y. Chen, and J. M. Lawrence, Phys. Rev. Lett. **97**, 097204 (2006).
[9] D. P. Rojas, L. Fernandez Barquin, J. I. Espeso, J. Rodriguez Fernandez, and J. Chaboy, Phys. Rev. B **78**, 094412 (2008).
[10] G. F. Zhou and H. Bakker, Phys. Rev. B **52**, 9437 (1995).
[11] J. S. Kim, G. R. Stewart, and K. Samwer, Phys. Rev. B **79**, 165119 (2009).
[12] E. V. Sampathkumaran, K. Mukherjee, K. K. Iyer, N. Mohapatra, and S. D. Das, J. Phys.: Condens. Matter. **23**, 094209 (2011).
[13] K. Mukherjee, K. K. Iyer, and E. V. Sampathkumaran, Solid State Commun. **152**, 606 (2012).
[14] C. Laubschat, E. Weschke, C. Holtz, M. Domke, O. Strebel, and G. Kaindl, Phys. Rev. Lett. **65**, 1639 (1990).
[15] *Perturbed Angular Correlations*, edited by E. Karlsson, E. Matthias, and K. Siegbahn (North-Holland, Amsterdam, 1964).
[16] G. Schatz and A. Weidinger, *in Nuclear Condensed Matter Physics* (Wiley, New York, 1996).
[17] E. Karlsson, *Solid State Phenomenon As Seen by Muons, Protons and Excited Nuclei* (Clarendon, Oxford, 1995).
[18] S. Cottenier, S. N. Mishra, S. Demuynck, J. C. Spirlet, J. Meersschaut, and M. Rots, Phys. Rev. B **63**, 195103 (2001).
[19] J. M. Lawrence, P. S. Riseborough, and R. D. Parks, Rep. Prog. Phys. **44**, 1 (1981).
[20] J. Aarts, F. R. de Boer, P. F. de Chatel, and A. Menovsky, Solid State Commun. **56**, 623 (1985).
[21] J. M. Lawrence, J. D. Thompson, and Y. Y. Chen, Phys. Rev. Lett. **54**, 2537 (1985).
[22] A. P. Murani, A. Severing, and W. G. Marshall, Phys. Rev. B **53**, 2641 (1996).
[23] Q. Wang and G. S. Collins, Hyperfine Interact., doi: 10.1007/s10751-012-0686-4.
[24] N. J. Stone, At. Data Nucl. Data Tables **90**, 75 (2005).
[25] B. E. Warren, *X-Ray Diffraction* (Addison-Wesley, Reading, MA, 1969), p. 251.
[26] Y. H. Lin, C. R. Wang, C. L. Dong, M. N. Ou, and Y. Y. Chen, J. Phys.: Conf. Ser. **273**, 012041 (2011).
[27] G. C. Carter, L. H. Bennet, and D. J. Kahan, in *Metallic Shifts in NMR, Progress in Material Science*, Vol. 20 (Pergamon Press, New York, 1977), Part I, p. 1.
[28] See, for instance, A. Sundaresan, R. Bhargavi, N. Rangarajan, U. Siddesh, and C. N. R. Rao, Phys. Rev. B **74**, 161306(R) (2006); C. Sudakar, P. Kharel, G. Lawes, R. Suryanarayanan, R. Naik, and V. M. Naik, Appl. Phys. Lett. **92**, 062501 (2008).
[29] J. P. Perdew, K. Burke, and M. Ernzerhof, Phys. Rev. Lett. **77**, 3865 (1996).
[30] P. Blaha, K. Schwarz, G. K. H. Madsen, D. Kvasnicka, and J. Luitz, *WIEN2K: An Augmented Plane Wave + Local Orbitals Program*

for Calculating Crystal Properties (Karlheinz Schwarz, Technische Universität, Wien, Austria, 1999).

[31]For the calculations presented here, we have used atomic sphere radii $R_{mt} = 2.5$ a.u for Ce and Pd. The maximum multipolarity inside the atomic sphere was restricted to $l_{\max} = 10$ and the plane-wave expansion was done with cutoff wave vector $K_{\max} = 8.0\,\text{a.u}^{-1}$. The k-point sampling was carried out with a dense k mesh of $20 \times 20 \times 20$ in the irreducible part of Brillouin zone and self-consistency was ascertained with energy and charge convergence criteria set to 1×10^{-6} Ry and 10^{-4}, respectively. For GGA + U calculations we have used $U = 6.2$ eV and $J = 0.7$ eV following Ref. 33.

[32]A. T. Burkov, E. Bauer, E. Gratz, R. Rasel, T. Nakama, and K. Yagasaki, Phys. Rev. B **78**, 035101 (2008).

[33]D. van der Marel and G. A. Sawatzky, Phys. Rev. B **37**, 10674 (1987).